Article

Combining Smartphone Inertial Sensors and Machine Learning Algorithms to Estimate Power Variables in Standing Long Jump

Beatrice De Lazzari [1,2,3], Giuseppe Vannozzi [1,2,*] and Valentina Camomilla [1,2]

[1] Department of Movement, Human and Health Science, University of Rome "Foro Italico", Piazza Lauro de Bosis 6, 00135 Roma, LZ, Italy; beatrice.delazzari@uniroma4.it (B.D.L.); valentina.camomilla@uniroma4.it (V.C.)

[2] Interuniversity Centre of Bioengineering of the Human Neuromusculoskeletal System, University of Rome "Foro Italico", Piazza Lauro de Bosis 6, 00135 Roma, LZ, Italy

[3] GoSport s.r.l., Via Basento, Lazio, 00198 Roma, LZ, Italy

* Correspondence: giuseppe.vannozzi@uniroma4.it

Abstract: Standing long jump (SLJ) power is recognized as informative of the ability of lower limbs to exert power. The study aims to provide athletes/coaches with a simple and low-cost estimate of selected SLJ power features. A group of 150 trained young participants was recruited and performed a SLJ task while holding a smartphone, whose inertial sensors were used to collect data. Considering the state-of-the-art in SLJ biomechanics, a set of features was extracted and then selected by Lasso regression and used as inputs to several different optimized machine learning architectures to estimate the SLJ power variables. A Multi-Layer Perceptron Regressor was selected as the best-performing model to estimate total and concentric antero-posterior mean power, with an RMSE of 0.37 W/kg, $R^2 > 0.70$, and test phase homoscedasticity (Kendall's $\tau < 0.1$) in both cases. Model performance was dependent on the dataset size rather than the participants' sex. A Multi-Layer Perceptron Regressor was able to also estimate the antero-posterior peak power (RMSE = 2.34 W/kg; $R^2 = 0.67$), although affected by heteroscedasticity. This study proved the feasibility of combining low-cost smartphone sensors and machine learning to automatically and objectively estimate SLJ power variables in ecological settings.

Keywords: SLJ; IMU; accelerometer; prediction; in-field test; ML

1. Introduction

The standing long jump (SLJ) is a sports-related movement widely employed for several aims: upper and lower body muscular fitness [1,2], anaerobic power [3,4], efficacy of a training intervention [5,6]; as a screening tool for athletes at increased risk of injury [7], to determine muscle imbalance [8]. Its role in the assessment of children's motor competence [9], talent identification [10], and prediction of player performance in different player positions [11] has also been investigated. As a recognized functional test, the SLJ allows for the analysis of the coordinated development of lower-body forces in the horizontal direction as a proxy for sprint performance in running [12,13] or in team sports such as American football [11] or rugby [5,6,10].

The SLJ is also used in conjunction with other tasks, such as the countermovement jump (CMJ) [14], to assess lower limb muscular strength in sports-related disciplines. In this last domain, both SLJ and CMJ are often part of athletic training because they represent an explosive type of motor task. For certain power-oriented athletic performances, such as ski jumping distance, the SLJ, which entails horizontal jumping ability, maybe a more effective motor task than the vertical one for both training and monitoring improvement [15].

Despite SLJs wide potential, all of these studies were limited to the simple and ecological assessment of the jumped distance (meter-based), with only a few studies characterizing the power of the jump using laboratory instrumentation [16–20]. However, laboratory-based measures are not applicable in the field, besides requiring expert operators and technical instrumentation. Meter-based assessments, while adequate for the sporting context, are limited in their ability to characterize power. A single study estimated SLJ total power using a stepwise multiple regression model that included only anthropometric features and jumped distance as independent variables [4]. Inertial measurement units (IMUs) are currently and regularly used as a viable solution for biomechanical analysis in an ecological setting, allowing for cost savings, increased portability, and outdoor data collection, hence boosting ecological validity [21]. Building on the research group's legacy [22] and on the state of the art [23], some attempts have been made to instrument jumping tasks such as CMJ [24,25] and SLJ [9] with smartphones. However, the cost of IMUs is not always affordable, and simple assessments, such as those meter-based, are still preferred in ecological settings, preventing users from the benefits of IMU-related knowledge [21].

In recent years, some attempts were made to create a cost-effective alternative to IMUs, leveraging the intrinsic capabilities of smartphones (SPs), which natively embody IMUs [21,24,26]. Although these sensors were not developed initially for biomechanical analysis and do not always meet the required specifications, such as high sampling frequency (>100 sample/s) or appropriate full-scale range (depending on the application), applications based on IMUs embedded in smartphones (SPs) are being developed to provide coaches with low-cost information [24,26,27]. To overcome the limitations of SP sensors, machine learning (ML) approaches have been proposed to enhance the quality of results comparable to those obtained with more reliable instruments [28]. To facilitate coaches' interpretation of obtained results related to jump performance, this research group has opted to embed biomechanical knowledge into ML models to estimate the outputs of interest [24,26] by identifying features that are more predictive of the outcome and could be given greater attention. As demonstrated by White et al. [25] on the CMJ task, the combination of discrete and continuous features extracted from IMU signals can help in estimating the output of interest; the two approaches together can improve the estimation in machine learning algorithms with respect to their separate use.

The aim of this research is to use IMUs integrated into smartphones and machine learning algorithms to estimate parameters that describe the power of SLJ, both overall and along the antero-posterior (AP) and vertical (V) directions separately. Predictors were selected that can be easily understood and employed by trainers, thereby facilitating the interpretability of the proposed ML solutions. To this end, non-categorical biomechanical features associated with the SLJ technique and intrinsic anthropometric characteristics are used to train and test selected optimizable ML architectures. Biomechanical features were selected based on two assumptions: (i) During the preparation phase, the SLJ vertical acceleration is similar to that expressed during a CMJ, given the presence of an eccentric and a concentric phase in both jumps, despite the differing muscle coordination patterns; (ii) during the flight phase, the origin of the sensor coordinate system follows a parabolic trajectory. Based on the identified features, several ML architectures dedicated to regression analysis were selected, and relevant models were trained, optimized, and tested. The dependency of the model performance on the participant's sex was also assessed.

2. Materials and Methods

2.1. Experimental Setup

One hundred fifty healthy sports science students were recruited to participate in the study (75 M, 75 F; mean ± SD: age = 22.3 ± 4.7 years; stature = 1.75 ± 0.12 m;

mass = 67.7 ± 10.9 kg). Only physically active participants were included, excluding from the study individuals who had undergone either lower limb surgery or injury in the six months prior to the experimental session. Prior to participating in the study, all participants provided written informed consent prior to the experimental session. The study was approved by the local Internal Review Board (No. CAR_94_2021_Rev2022).

Participants held an SP in their right hand, as depicted in Figure 1 (Samsung Galaxy S9+, Samsung Group, Seoul, Republic of Korea; sampling frequency = 500 samples/s; full-scale range: accelerometer = ± 8 g; gyroscope = ± 500 deg/s). The app Phyphox v.1.1.16 was used to acquire all SP-IMU data [29], which was remotely controlled from the laboratory PC. Prior to each experimental session, the SP-IMU was calibrated, as detailed in the "Data processing of force plate and SP-IMU signals" section. Subsequently, each participant received instructions on the correct execution of a standing long jump (SLJ), and following a familiarization phase, they performed three trials in accordance with the operator's directives. Jumps were executed with the left hand on the hip and the right one near the hip while holding the SP horizontally (Figure 1). The participant performed the jumps starting from a force plate (Bertec, Bertec Corporation, Columbus, OH, USA; sampling frequency = 1000 samples/s; size = 40 × 40 cm) to extract the ground reaction force (GRF) signals necessary to calculate the jump power. Holding the arms still allows the SP to remain in a steady position near the hip, which is crucial for segmenting the jump into the three following phases: (i) a brief static phase in which the participant is ready to jump with hands on the hips, feet in a parallel stance, and heels at the zero of a meter tape; (ii) a vocal command that triggers the jumping trial; and (iii) a second static phase after landing. The jump was considered correct if the participant was able to maintain equilibrium after landing without realizing an additional step, with the feet in the parallel stance position and the arms still. The meter tape was used to measure the heel-to-heel jump distance, which was used as one of the features to estimate the jump power.
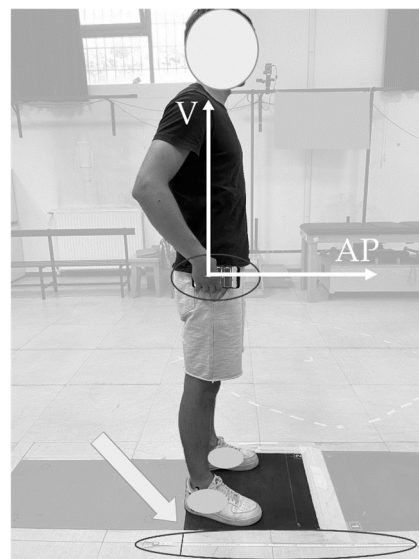
Figure 1. Experimental setup. Before the jump, the participant assumes the akimbo style pose over the force plate, with the SP in their right hand. The arms are maintained fixed with the hip (small black ellipse). The tape meter (big black ellipse) has the zero (highlighted with a black sign and a white arrow) near to the right heel, which corresponds to the initial position.

To reach the aim of this work, the workflow presented in Figure 2 was used:
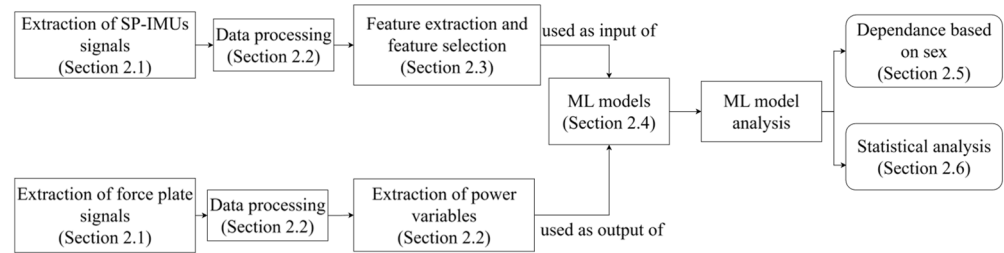
Figure 2. Workflow of the process to estimate power variables using a machine learning (ML) approach combined with SP-IMUs signals. The flowchart represents the steps from extraction of signals (SP-IMUs and force plate, Section 2.1) to machine learning models (ML models, Section 2.4), with analysis of the optimized models (Sections 2.5 and 2.6).

2.2. Data Processing of Force Plate and SP-IMU Signals

Force plate and SP-IMUs signals were processed using MATLAB R2022a (The MathWorks Inc., Natick, MA, USA).

For each jump acquired through the force plate, the GRF was acquired and filtered using a 2nd order low-pass Butterworth filter with a cut-off frequency of 50 Hz.

Prior to each experimental session, the SP-IMUs were calibrated to compute and eventually correct their offset and cross-axis sensitivity. Following the approach outlined in [30], a 60-second static trial was acquired with the SP positioned on a flat surface to determine and then remove the gyroscope static bias, calculated as the mean value of the static trial, from each subsequent jump measure. Subsequently, three ad hoc 60-second static acquisitions of the accelerometer were conducted, each acquisition involving the alignment of one of the three accelerometer axes with the gravity vector direction [30]. To ensure a consistent gravity removal, acceleration measures were expressed in the global coordinate system using quaternions, obtained from gravity and the plane of action. This was carried out under the hypothesis that the smartphone was kept parallel to the plane of movement to avoid the need for an accurate estimate of its yaw [31].

For each jump that was successfully acquired, selected quantities were computed from the preprocessed force plate and SP-IMUs signals as described in Table 1.

Table 1. Variables' calculation using force plate signals or SP-IMU signals. Details on symbols and legend are in the footer.

Step	Variable	How to Calculate	
		Force plate signals	SP-IMU signals
1	M	Mean value of the force vertical component in the first two seconds of the static phase ($GRF_{V,static}$) divided by gravity acceleration (g = 9.81 m/s^2): $m = \frac{mean(GRF_{V,static})}{g}$	-
2	$a_{CoM,V}$ and $a_{CoM,AP}$	$a_{CoM,V} = \frac{GRF_V - mean(GRF_{V,static})}{m}$ $a_{CoM,AP} = \frac{GRF_{AP}}{m}$	Hp: the smartphone is kept parallel to the plane of movement during the task execution, i.e., the yaw is not changing [24,26,31] Vertical (a_V) and anteroposterior (a_{AP}) acceleration components of the acceleration expressed into the global coordinate system

Table 1. *Cont.*

Step	Variable	How to Calculate	
3	t_0 and t_{TO}	t_0: onset identified as the time frame occurring 30 ms prior the first sample deviating by 8 times the standard deviation of the static phase of $a_{CoM,V}$, similarly to [32]. t_{TO}: take-off identified as the first frame such that $a_{CoM,V} \leq -g$.	t_0 and t_{TO} defined on a_V as with the force plate data, and similarly to [32]
4	$v_{CoM,V}$ and $v_{CoM,AP}$	$v_{CoM,V} = \int_{t_0}^{t_{TO}} a_{CoM,V}$ $v_{CoM,AP} = \int_{t_0}^{t_{TO}} a_{CoM,AP}$ Integration interval from t_0 to t_{TO} to minimize the noise contribution linked to the drift effect	$v_V = \int_{t_0}^{t_{TO}} a_V$ $v_{AP} = \int_{t_0}^{t_{TO}} a_{AP}$
5	t_{UL} and t_{UB}	-	t_{UL}: time of minimum of vertical acceleration after the jump onset t_{UB}: time of minimum vertical velocity
6	t_{BP}	It is the instant in which the vertical velocity $v_{CoM,V}$ crosses 0.	Identified as instant of time when the vertical velocity v_V crosses 0.
7	P_V and P_{AP}	$P_V = GRF_V * v_{CoM,V}$ (1) $P_{AP} = GRF_{AP} * v_{CoM,AP}$ (2)	-
8	P_{TOT}	Hp: medio-lateral contribution is negligible for the type of the jump $P_{TOT} = \sqrt{P_V^2 + P_{AP}^2}$ (3)	-
	What is extracted? Why?		**What is extracted? Why?**
	Mean and peak values of P_{TOT}, P_V, P_{AP} to be used as outputs to be estimated using machine learning		Biomechanical features (Presented in Section 2.3) used as inputs of machine learning models to estimate the force plate quantities

Legend: m—mass of the participant; $a_{CoM,V}$ and $a_{CoM,AP}$—the acceleration of the center of mass (CoM) for the vertical (V) and antero-posterior (AP) directions; t_0 and t_{TO}—onset and take-off instants; $v_{CoM,V}$ and $v_{CoM,AP}$—vertical and antero-posterior components of velocity of CoM; t_{UL} and t_{UB}—unloading instant of time and eccentric yielding instant of time; t_{BP}—jump braking onset instant; P_V and P_{AP}—vertical and antero-posterior power profiles; P_{TOT}—total power profile.

The variables and time instants listed in Table 1 are depicted in the following plots of force plate and SP-IMU signals, to ease understanding.

The power and CoM acceleration exerted along the vertical and antero-posterior components during the static and preparation phases of the jumps, as acquired using force plates, are reported in Figure 3.
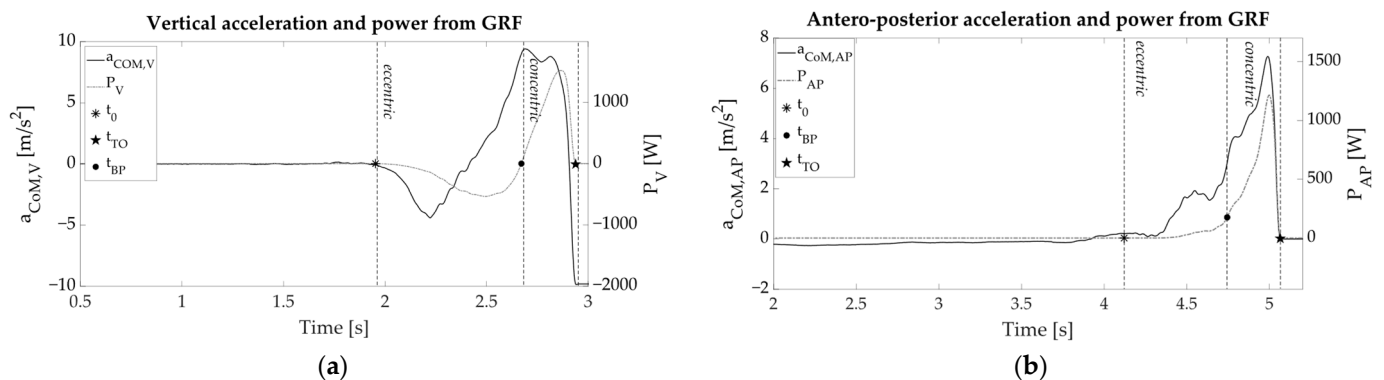

(a)   (b)

Figure 3. Ground Reaction Force (GRF) derived: (**a**) vertical component of the acceleration ($a_{CoM,V}$) and power (P_V); (**b**) antero-posterior component acceleration ($a_{CoM,AP}$) and power (P_{AP}). Dashed vertical lines define the concentric (from t_0 to t_{BP}) and eccentric phases (from t_{BP} to t_{TO}).

The preparation phase of the SLJ in its vertical component (Figure 3a) is comparable to that of the CMJ [33]. Therefore, it was segmented into two phases: eccentric and concentric. The eccentric phase starts from the onset time (t_0), while the concentric one ends with the take-off (t_{TO}). The time instant at which the eccentric and concentric phases are divided is the breaking time instant, defined as the time in which $v_{CoM, V}$ crosses zero, t_{BP}.

The power variables of interest were extracted from the force data in the following time intervals: mean and peak concentric power of P_{TOT}, P_V, and P_{AP}, between braking time and takeoff; mean power of P_{AP}, between onset time and takeoff (Table 2). Power variables were normalized to the mass of the participant to be mass independent (W/kg).

Table 2. List of the power variables calculated from the force plate signals, reported with their acronym (ID), corresponding description, and time interval for the determination. All features are normalized with respect to the mass of the participant.

ID	Variable (W/kg)	Time Interval
$P_{TOT, peak}$	Positive P_{TOT} peak in the take-off phase	$t \in [t_0, t_{TO}]$
$P_{TOT, conc}$	Mean concentric P_{TOT} power	$t \in [t_{BP}, t_{TO}]$
$P_{V, peak}$	Positive P_V peak in the take-off phase	$t \in [t_0, t_{TO}]$
$P_{V, conc}$	Mean concentric P_V power	$t \in [t_{BP}, t_{TO}]$
$P_{AP, peak}$	Positive P_{AP} peak in the take-off phase	$t \in [t_0, t_{TO}]$
$P_{AP, conc}$	Mean concentric P_{AP} power	$t \in [t_{BP}, t_{TO}]$
$P_{AP, tot}$	Mean P_{AP} power in the take-off phase	$t \in [t_0, t_{TO}]$

Legend: P_V and P_{AP}: vertical and anteroposterior components of power; t_0 = jump onset; t_{TO} = jump takeoff, t_{BP} = jump braking. All features are measured in W/kg.

Regarding the analysis of SP-IMU signals, the SLJs preparation phase was subdivided into eccentric and concentric phases, as previously conducted for force plate signals. Further subphases were also considered in accordance with [16] (Figure 4): the unloading phase, defined as the time between the jump onset (t_0) and the instant at which the vertical acceleration reaches the minimum (t_{UL}); the eccentric yielding phase starting at t_{UL} and ending when vertical velocity reaches the minimum (t_{UB}); the eccentric braking phase defined as the time between t_{UB} and when the vertical velocity crosses 0 (t_{BP}); and the concentric propulsive phase as the time between t_{BP} and the take-off (t_{TO}). These phases are useful to define some of the features analyzed in the following section. The calculations of these time instants are reported in Table 1.

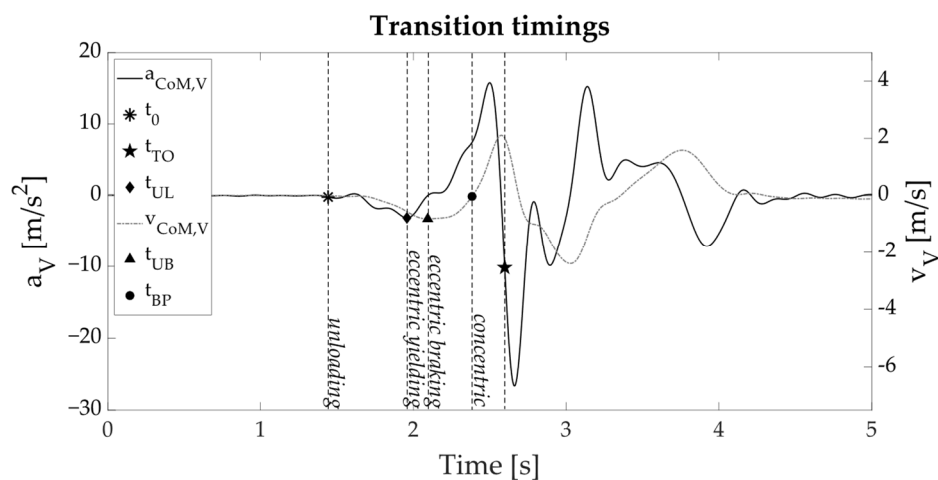**Figure 4.** Vertical acceleration (a_V) and velocity (v_V) extracted from SP-IMUs with highlighted phases: unloading ($t_0 - t_{UL}$), eccentric yielding ($t_{UL} - t_{UB}$), eccentric braking ($t_{UL} - t_{BP}$), and concentric propulsive phase ($t_{BP} - t_{TO}$). Legend for time instants: t_0 = jump onset; t_{UL} = minimum acceleration; t_{UB} = minimum velocity; t_{BP} = velocity crosses 0; t_{TO} = take-off.

2.3. Feature Selection

In Table 3, the sixty-one features extracted from SP-IMUs signals are reported.

Table 3. Proposed features with the indication of their acronym (ID), measurement unit, and brief description. Details on symbols and legend are in the footer.

	ID	Feature	Measurement Unit	Description
Subject related	h_{anthro}	Participant's stature	m	-
	w_{anthro}	Participant's body mass	kg	-
	y_{anthro}	Participant's age	y	-
	l_{meter}	Length of the jump measured with tape meter	m	-
Mann	$P_{power, Mann}$	Peak of the total power	W	$P_{power, Mann} = 32.49 * l_{meter} + 39.69 * w_{anthro} - 7.608$
	$A_{power, Mann}$	Average of the total power	W	$A_{power, Mann} = 28.31 * l_{meter} + 30.03 * w_{anthro} - 7.408$
Biomechanical	h_{jump}	Ballistic SLJ maximal height	m	$h_{jump} = \frac{(v_V(t_{TO}))^2}{2*g}$
	A_V	Unweighting phase duration	s	$[t_0, t_{UB}]$
	b *	Minimum acceleration	m/s²	$a_V(t_a^V{}_{\_min})$
	C *	Time interval from minimum to maximum acceleration	s	$[t_{a*\_min}, t_{a*\_max}]$
	Δa *	Range between min-to-max acceleration in the time between t_0 and t_{TO}	m/s²	$\Delta a^* = max(a^*(t_0 \div t_{TO})) - min(a^*(t_0 \div t_{TO}))$
	Δv *	Range between min-to-max acceleration in the time between t_0 and t_{TO}	m/s	$\Delta v^* = max(v^*((t_0 \div t_{TO})) - min(v^*(t_0 \div t_{TO}))$
	D *	Main positive impulse time duration	s	Time duration of positive acceleration in a * signal in the time interval $[t_0, t_{TO}]$
	E *	Maximum acceleration	m/s²	$a^*(t_a^*{}_{\_max})$
	F *	Time interval from acceleration positive peak to the take-off	s	$[t_{a*\_min}, t_{TO}]$
	G_V	Ground contact duration	s	$[t_0, t_{TO}]$
	H *	Time interval from minimum acceleration to the end of the eccentric braking phase	s	$[t_{UL}, t_{BP}]$
	i_V	Maximum positive slope of a_V	m/s²	$i_V = max\left(\frac{d(a_V(t))}{dt}\right) t \in [t_0, t_{BP}]$
	J *	Time duration from the negative peak velocity to the end of the eccentric braking phase	s	$[t_{v*\_min}, t_{BP}]$
	K *	Acceleration at the end of the eccentric breaking phase	m/s²	$a^*(t_{BP})$
	L *	Negative peak power	W/kg	$P(t_{P*\_max})$
	L_{AP}	Time duration between the min and max values in the range $[t_0 \div t_{TO}]$	s	$[t_P^{AP}{}_{\_min}, t_P^{AP}{}_{\_max}]$
	M *	Eccentric positive power duration	s	-
	n *	Positive peak power	W/kg	$P(t_{P*\_min})$
	O *	Time duration between positive peak power and take-off	s	$[t_{P*\_max}, t_{TO}]$
	p *	Mean slope between acceleration peaks	a.u.	$p^* = \frac{e^*-b^*}{C^*}$
	q *	Shape factor	a.u.	Ratio between the area under the curve from t_{UB} to the last positive sample prior t_{TO} (lasting D*) and the one of a rectangle of sides D* and e*
	Q_V	Time duration between the eccentric braking phase and the take-off	s	$[t_{BP}, t_{TO}]$
	r *	Impulse ratio	a.u.	$r^* = \frac{b^*}{e^*}$
	R_{AP}	Entire positive power duration in the AP component	s	-
	u *	Mean concentric power	W/kg	Average value of $P^*(t)$, $t \in [t_{BP}, t_{TO}]$
	v *	Minimum negative velocity	m/s	$v^*(t_{v*\_min})$
	W *	Time duration between minimum and maximum power instants	s	$[t_{P*\_min}, t_{P\_max}]$
	z *	Mean eccentric power	W/kg	Average value of $P^*(t)$, $t \in [t_0, t_{BP}]$

Table 3. *Cont.*

	ID	Feature	Measurement Unit	Description
Time-frequency	f1 *	High central frequency	Hz	Highest VMD central frequency, associated with wobbling and noise
	f2 *	Middle central frequency	Hz	Middle VMD central frequency, associated with wobbling tissues
	f3 *	Low central frequency	Hz	Lower VMD central frequency, associated with the jump proper

Subscripts and superscripts: "V" and "AP" subscripts, related to vertical and anteroposterior components of velocity/acceleration; "*" superscript, used when the features are extracted from both AP and V components; "anthro" subscript, used for anthropometric features. Time intervals are indicated with capital letters, while other features are reported with small letters. Features are grouped by type and alphabetically sorted. Legend: a.u. = arbitrary units; time instants: t_0 = jump onset; t_{a_min} = minimum acceleration; t_{a_max} = maximum acceleration; t_{v_min} = minimum velocity; t_{P_min} = minimum power; t_{P_max} = maximum power; t_{TO} = jump takeoff; t_{UL} = jump unloading; t_{BP} = jump braking.

More in detail, 6 were obtained from basic measurements:

- Three were related to the anthropometric characteristics of the subject (indicated using "anthro" subscript): stature, mass, and age.
- Jump length (l_{meter}) was obtained by measuring the heel-to-heel distance taken from the meter tape.
- Two variables were computed following the work of Mann [4]: namely, peak power ($P_{Power,Mann}$) and average power ($A_{Power, Mann}$), starting from mass and jumped distance.

Further 55 features were obtained from either a_V, a_{AP}, or both, as they both contribute to the SLJ power estimate.

- SLJ maximal height (h_{jump}), hypothesizing that the trajectory of the origin of the sensor coordinate system during a SLJ can be approximated to a ballistic motion. From the acceleration signals, the vertical velocity at take-off is extracted and then used to this aim (Table 3).
- Twenty-one jump-related features were calculated twice for both V and AP components, reported with *, whereas eight features were calculated for a single component—reported with "V" or "AP" subscripts. Features from A to R and v were inspired by [34]; u, W, and z enriched the description of power-related variables as presented in [24].
- Six time-frequency features were obtained by processing a_V and a_{AP} via Variational Mode Decomposition (VMD) [35], by subdividing the signal into N intrinsic mode functions, each having a frequency spectrum centered around a central frequency. In this case, N was set to 3, with f1 and f2 (namely, the high- and mid-central frequencies) assumed to be potential descriptors of wobbling or artifacts due to involuntary arm movements; f3 (the low-central frequency) associated with the jump itself [24].

2.4. Model Generation and Evaluation in the Whole Dataset

After data filtering and feature extraction, each of the 450 jumps was analyzed to obtain a record including the abovementioned 61 features, leading to the final dataset (450×61). The same dataset composed of 61 features was used to estimate the seven possible power outputs as identified in Table 2.

The dataset was separated as follows: 80% of the participants (120 subjects, 60 M, and 60 F, for a total of 360 jumps) were used as the training set, and the remaining 20% (30 subjects, 15 M, and 15 F, for a total of 90 jumps) were used as the test set. The creation of the two sets was entrusted to a randomization algorithm that considered the sex of the subject to have an equal distribution of both males and females in training and test sets. Moreover, the training set and test set were designed to be independent of each other, not

including in the test set any of the jumps belonging to a subject of the training set and vice versa.

Prior to the training phase, the features of the training set were normalized through z-score transformation. For each output to be estimated, the feature number was then reduced through Lasso regularization. The regularization strength was fixed at $\alpha = 0.1$ to avoid possible multicollinearity among features [36]. The resulting subset of features was then used to develop the ML models.

The final datasets, composed of selected features and related outputs, were exported from MATLAB to be used in Jupyterlite Notebook (v. 0.5.0), a Python environment. In Jupyter Notebook, ML models were optimized using the GridSearchCV function, which can handle several inputs:

- The cross-validation criterion, which is used to validate the model. Among the options, the GroupKFold (with K = 5) cross-validation method was selected to internally consider training subjects and validation subjects as separate entities and to prevent data leakage [37].
- The processing step, which is used to process data before optimization. The not-normalized training set was combined with the PowerTranformer() function to correctly scale the training and validation sets in every fold to prevent data leakage.
- The list of hyperparameters to be optimized, with the relative ranges of values.
- The selection criterion of the model. Mean absolute error (MAE) was used to select the best configuration of hyperparameters.

The following regression models were trained, taken from the scikit-learn module:

- Tree and Random Forest (RF) were considered because they are simpler to implement than other models in the perspective of developing the model inside the smartphone.
- Optimized support vector regressor (SVR) was evaluated as a general and good solution found in the literature [38].
- Optimized ensembles (ADA Boost Regressor (ADABR), Gradient Boosting Regressor (GBR), Histogram-based Gradient Boosting Regression Tree (HGBR), XGBoost Regressor (XGBR)): these solutions are typically used for limited datasets of interest.
- Optimized Gaussian Process Regression (GPR) and optimized Multi-Layer Perceptron Regressor (MLPRs): these models proved to be effective solutions for similar problems: SLJ length estimation, and CMJ height estimation respectively [24,26].

For each selected architecture, Table A1 reports the list of hyperparameters to be optimized using the Grid Search optimization method.

For each trained model, the following metrics were computed for both training and test sets: the root-mean-square error (RMSE), mean squared error (MSE), mean absolute error (MAE), and R^2.

After training, the best model for each architecture was selected based on the minimum mean absolute error (MAE) and used in the subsequent test phase. To perform the test phase of the optimized models, the normalizing factors of the training set were used to normalize the test set.

After testing, a final model for each output variable was chosen based on the lowest RMSE value.

The models that showed valuable results were evaluated in terms of heteroscedasticity [39] to select those able to estimate the output with an error independent from the measured quantity.

For models demonstrating adequate performance and homoscedasticity, an additional analysis was performed to assess the extent to which each input variable influences the estimate and contributes to the interpretation of the model. To this aim, a permutation

feature importance (PFI) analysis [40–42] was carried out on the training set. PFI is an iterative procedure that analyzes the change of the model MSE error when each input variable is randomly permuted and the others are maintained as they are. For each variable, an index can be calculated, defined as the ratio between the MSE obtained after the permutation of the i-th input variable (MSE_i) and the MSE of the model without any permuted variables (MSE_0). A higher ratio corresponds to a higher contribution of the i-th variable to the estimate, and vice versa.

2.5. Model Dependance from Participants' Sex

To assess if the ML model output was dependent on the participant's sex, the procedure described in Section 2.5 was replicated on two separate sub-datasets, each comprising seventy-five participants of each sex (225 jumps). For these datasets, the division between training and test sets was not performed to avoid further reduction of the dataset. However, the cross-validation phase was maintained using GridKFold, as was carried out for the entire dataset. The ML architectures presented in Table A1 were verified for all the estimated output power variables of interest.

To attribute potential performance differences of the sex-specific models with respect to those obtained from the overall dataset to sex or dataset size, the same procedure was repeated using a mixed dataset composed of an overall number similar to the sex-separated dataset (and divisible by 5), balanced for male/female subjects (80 participants, 40 M, 40 F).

2.6. Statistical Analysis

Regarding the models obtained using the whole dataset, the best model for each architecture was analyzed on the test data using Bland and Altman plots [39]. To realize Bland and Altman plots, the following elements were computed:

- upper limit UL = BIAS + 1.96 * SD;
- lower limit LL = BIAS − 1.96 * SD
- BIAS = test value − model predicted value
- SD = standard deviation of the previous difference
- confidence intervals (CI) at 95% of BIAS, UL, and LL following [43] and based on *t*-value, number of samples in the test set (n), and standard error for the BIAS (SE_{BIAS}).

Bland and Altman plots are generated, including confidence intervals, the regression line of the averages vs. the differences of the estimated and real variables (characterized by the coefficient and intercept value and the associated R_{AB}^2). The presence of data heteroscedasticity was verified by calculating Kendall's τ coefficient [44] (in case of $\tau > 0.1$).

Furthermore, the performance of each model was analyzed through the following three metrics applied to the test set: (i) accuracy, obtained as the RMSE between the reference value and the estimated one; (ii) precision, calculated as the standard deviation of the distance between the reference and estimated values; (iii) bias, defined as the mean distance between the reference values and the estimated ones.

Regarding models obtained using the subsets, the same metrics used for the entire dataset were evaluated to investigate and quantify whether the model can perform differently depending on sex and/or the limited amount of data.

3. Results

The 450 jumps had the following values for each output variable (Table 4):

Table 4. The values of the presented features calculated in the population of interest, considering all the 450 jumps: range, minimum, and maximum values: power values are normalized with respect to the mass of the participant of interest.

ID	Ranges [W/kg]	Minimum Value [W/kg]	Maximum Value [W/kg]
$P_{TOT,\ peak}$	30.6 ± 5.9	10.7	53.8
$P_{TOT,\ conc}$	4.3 ± 1.1	0.7	10.2
$P_{V,\ peak}$	28.7 ± 5.8	9.3	51.9
$P_{V,\ conc}$	3.9 ± 1.0	0.4	9.7
$P_{AP,\ peak}$	10.3 ± 3.8	2.3	21.1
$P_{AP,\ conc}$	1.5 ± 0.6	0.3	3.6
$P_{AP,\ tot}$	1.8 ± 0.7	0.3	3.8

The Lasso regularization led to selecting the following number of features out of 61 features available to train the ML models: 50 for $P_{TOT,\ peak}$; 48 for $P_{TOT,\ conc}$; 25 for $P_{V,\ peak}$; 26 for $P_{V,\ conc}$; 49 for $P_{AP,\ peak}$; 32 for $P_{AP,\ conc}$; 48 for $P_{AP,\ tot}$.

3.1. Model Creation and Evaluation in the Whole Dataset

The best model, as obtained by Grid Search optimization, is reported for each output variable in Table 5. For the same models, bias, accuracy, Kendall's tau, and sigma values calculated on the test set are reported in Table 6.

Table 5. For each output variable, the best model is reported that has the lowest RMSE value (train—test). Relevant functions and optimized hyperparameters are also listed. In bold, models that performed with an $R^2 > 0.6$.

Output Feature	Model	Hyperparameters	RMSE [W/kg]	MSE [(W/kg)²]	MAE [W/kg]	R^2
$P_{TOT,\ peak}$	GPR	Alpha: 0.1 Kernel: RationalQuadratic(alpha = 1, length_scale = 1) * 1 ** 2 Optimizer: Fmin_1_bfg_b	5.20–5.38	27.5–29.0	3.93–4.10	0.20–0.18
$P_{TOT,\ conc}$	None	-	-	-	-	-
$P_{V,\ peak}$	ADABR	Learning rate: 10^{-9} Loss: Square N_estimators: 135	5.34–5.54	29.0–30.7	3.97–4.12	0.12–0.07
$P_{V,\ conc}$	HGBR	Loss: absolute_error Learning rate: 0.17 Max_iter: 28 s	0.89–0.95	0.84–0.91	0.61–0.68	0.15–0.14
$P_{AP,\ peak}$	MLPR	Activation: identity Alpha: 10^{-4} LayerSize: 47 LearningRate: constant Solver: sgd	2.11–2.34	4.48–5.49	1.67–1.86	**0.68–0.67**
$P_{AP,\ conc}$	MLPR	Activation: identity Alpha: 10^{-3} LayerSize: 9 LearningRate: invscaling Solver: adam	0.28–0.37	0.08–0.13	0.22–0.29	**0.73–0.71**
$P_{AP,\ tot}$	MLPR	Activation: identity Alpha: 10^{-6} LayerSize: 24 LearningRate: adaptive Solver: sgd	0.31–0.37	0.09–0.14	0.25–0.30	**0.76–0.75**

Names of hyperparameters as reported in Jupyterlite Notebook, where the symbol "*" stands for a multiplication and "**" for the exponentiation.

Table 6. List of the parameters calculated for the best models for each output variable on the test set (models reported in Table 5). Kendall's tau τ < 0.1, indicated in bold, means homoscedastic data.

Output Feature	BIAS	KENDALL	ACCURACY	SIGMA
$P_{TOT, peak}$	0.09	−0.90	6.40	6.37
$P_{TOT, conc}$	-	-	-	-
$P_{V, peak}$	0.13	**0.03**	5.54	5.57
$P_{V, conc}$	−0.16	0.19	0.95	0.95
$P_{AP, peak}$	0.13	0.20	2.34	2.35
$P_{AP, conc}$	0.06	**0.04**	0.37	0.37
$P_{AP, tot}$	0.003	**0.09**	0.37	0.37

Among the optimized models reported in Table 5, only those for $P_{AP, peak}$, $P_{AP, conc}$, and $P_{AP, tot}$ variables showed R^2 > 0.6. The models for $P_{AP, conc}$, and $P_{AP, tot}$ were also homoscedastic, while the one for $P_{AP, peak}$ was heteroscedastic (Table 6).

3.2. Model Dependance from Participants' Sex

As illustrated in Table 7, the optimized models identified using reduced datasets (M, F, and half mixed) are able to estimate homoscedastic variables ($P_{AP, conc}$, and $P_{AP, tot}$). The optimized models identified for the remaining power variables using reduced datasets (M and F) are documented in Appendix A—Tables A2 and A3, respectively.

Table 7. List of the best models for $P_{AP, conc}$, and $P_{AP, tot}$ output variables using reduced datasets (M = only males, F = only females, Half mixed = 80 participants, 40 M, and 40 F) as input datasets in grid search optimization, with optimized hyperparameters and mean values of the metrics along the 5-folds.

Output Feature	Dataset Type	Model	Hyperparameters	RMSE [W/kg]	MSE [(W/kg)²]	MAE [W/kg]	R^2
$P_{AP, conc}$	M	MLPR	Activation: identity Alpha: 10^{-4} LayerSize: 30 LearningRate: invscaling Solver: adam	0.32	0.10	0.26	0.57
	F	GPR	Alpha: 10^{-1} Kernel: RBF (length_scale = 1) * 1 ** 2 Optimizer: fmin_l_bfgs_b	0.27	0.07	0.20	0.69
	Half mixed	MLPR	Activation: identity Alpha: 10^{-6} LayerSize: 30 LearningRate: invscaling Solver: adam	0.29	0.09	0.24	0.68
$P_{AP, tot}$	M	MLPR	Activation: identity Alpha: 10^{-5} LayerSize: 35 LearningRate: adaptive Solver: adam	0.35	0.13	0.28	0.59
	F	SVR	C: 0.3 Degree: 1 Epsilon: 10^{-3} Kernel: poly	0.26	0.07	0.19	0.71
	Half mixed	MLPR	Activation: identity Alpha: 10^{-1} LayerSize: 19 LearningRate: adaptive Solver: adam	0.32	0.11	0.26	0.72

Names of hyperparameters as reported in Jupyterlite Notebook, where the symbol "*" stands for a multiplication and "**" for the exponentiation.

3.3. Quality Model Analysis

The quality of the $P_{AP, tot}$, and $P_{AP, conc}$ MLRP models is represented in terms of Bland and Altman plots (Figure 5). Along with the values used to perform them (Table 8).
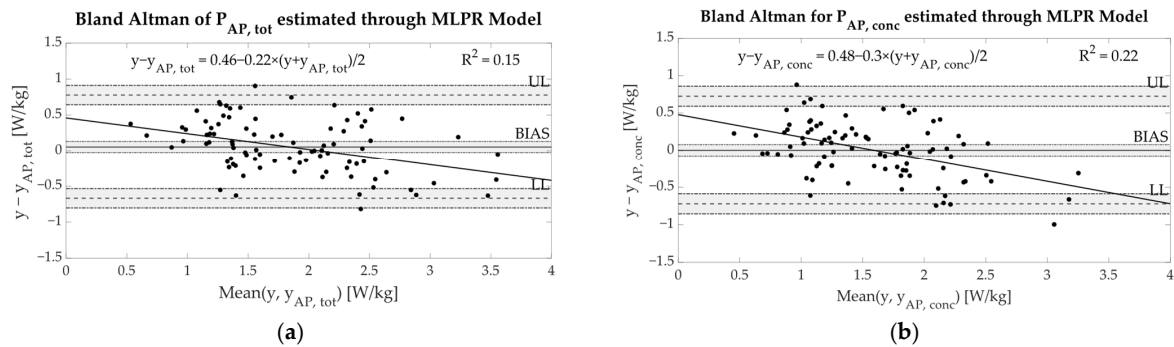

(a)

(b)

Figure 5. Bland-Altman plots on the test set: (**a**) $P_{AP, tot}$; (**b**) $P_{AP, conc}$. Legend: upper limit (UL = BIAS + 1.96 × SD), lower limit (LL == BIAS − 1.96 × SD), confidence intervals (CI) at 95% of BIAS, UL, and LL were calculated following [43], with BIAS = test value—model predicted value; SD = standard deviation of the previous differences. In both plots, the equation and R^2 show values lower than 0.3.

Table 8. Parameters used for each model: accuracy, precision, bias, UL, and LL of the difference are expressed in meters.

Parameter	MLPR $P_{AP, tot}$	MLPR $P_{AP, conc}$
Accuracy [m]	0.37	0.37
Precision [m]	0.37	0.37
Bias [m]	0.06	0.0028
CI_{BIAS} (95%) [m]	[−0.017 0.13]	[−0.075 0.08]
UL [m]	0.79	0.73
CI_{UL} (95%) [m]	[0.66 0.92]	[0.59 0.862]
LL [m]	−0.67	−0.7224
CI_{LL} (95%) [m]	[−0.80 −0.54]	[−0.59 −0.856]
Kendall's τ	0.06	0.09
Samples (n)	90	90
t-value	1.987	1.987
SE_{BIAS} ($s/\sqrt{n}$)	0.039	0.039

Data homoscedasticity can be inferred from Kendall's tau coefficient (τ) ($\tau < 0.1$). To allow calculations, samples (n); CI = Confidence Interval; t-value; SE_{BIAS} = standardized error of the estimates are also reported.

For $P_{AP, conc}$ and $P_{AP, tot}$ that showed ML good models and homoscedastic behavior, the PFI was performed using the training set (Figures 6 and 7, respectively).
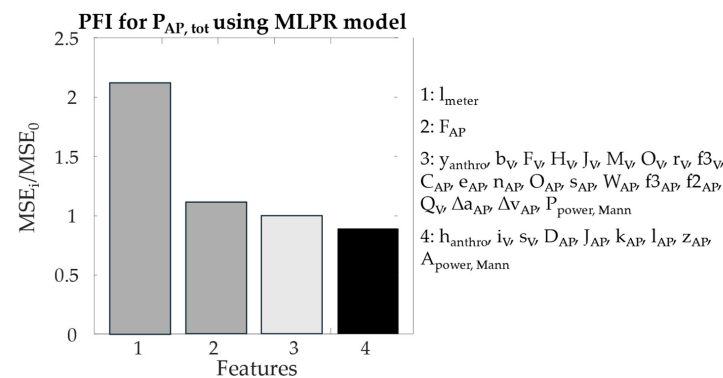

Figure 6. PFI performed on MLPR model used to estimate $P_{AP, tot}$. In the legend, the 32 features used to estimate $P_{AP, tot}$ divided into four groups in terms of PFI output. The first two groups (dark grey) showed an MSE_i/MSE_0 greater than 1, meaning that the features belonging to those groups affect the estimate of the output more. The third group (light grey) showed a MSE_i/MSE_0 equal to 1, while the fourth group (black) showed a MSE_i/MSE_0 lower than 1.
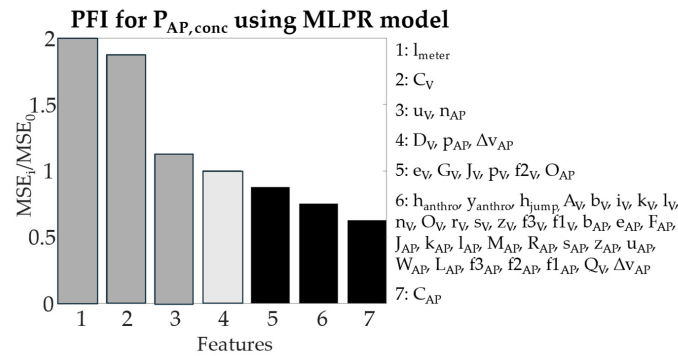
Figure 7. PFI performed on MLPR model used to estimate $P_{AP\,conc}$. In the legend, the 48 features used to estimate $P_{AP,\,conc}$ divided into seven groups in terms of PFI output. The first three groups (dark grey) showed an MSE_i/MSE_0 greater than 1, meaning that the features belonging to those groups affect the estimate of the output more. The fourth group (light grey) showed a MSE_i/MSE_0 equal to 1, while the black groups showed a MSE_i/MSE_0 lower than 1.

4. Discussion

This study demonstrated the efficacy of a combination of biomechanical features extracted from smartphone IMUs and machine learning techniques in estimating the power characteristics of a single-leg jump. Furthermore, it was shown that model performance was dependent on the dataset size rather than the participants' sex. Overall, this work highlights the potential for in-field use of this technology to monitor athletes directly.

The results of the estimation process demonstrated that the models of $P_{AP,\,tot}$, and $P_{AP,\,conc}$ produced meaningful estimations, whilst the performance of the other models was unsatisfactory. This discrepancy may be attributed to the varying ranges of the output variables (see Table 4), despite the dataset size remaining the same (450 trials in total), which can have an impact both on models' performance and heteroscedasticity.

With respect to the performance of the $P_{AP,\,tot}$, and $P_{AP,\,conc}$ models in the test phase, both best models were based on MLPR architectures and showed R^2 values higher than 0.70 (Table 5). These models also provided faster results compared to other architectures, such as GPR models. Moreover, the estimation was homoscedastic, indicating that errors in the estimates were not dependent on the measured quantities. It is important to note, on one side, that SP-IMUs are not specifically selected for biomechanical purposes, and on the other side, that current results relied on the highest possible SP-IMU sampling frequency available on the SP market (fs = 500 sample/s) to maximize data quality.

The features that were selected for the estimation of $P_{AP,\,tot}$ and $P_{AP,\,conc}$ included, in both cases, the jump length, l_{meter}, anthropometric data (subject height and age, h_{anthro} and y_{anthro}), and frequencies extracted using Variational Mode Decomposition (VMD).

Among related studies, the work by Mann et al. [4] appears to be the most similar to the present study, although direct comparison is complex. The models utilized in this present study are distinct from those employed by Mann et al. The current models are based on a more general population, a not-sport-specific population that is not limited to athletes and includes both sexes as well as a larger number of participants. Additionally, the predicted output differs between the studies. Nevertheless, the key features identified in the work of Mann et al. remain relevant as predictors of power outputs, with both anthropometric parameters and jump length selected as predictors after feature selection. Furthermore, the relationships established by Mann et al. contribute to the estimation of $P_{AP,\,tot}$, and $P_{AP,\,conc}$, suggesting that, despite differences in the populations, their findings offer a partial basis for the present estimates.

The PFI analysis indicated that, for both $P_{AP, tot,}$ and $P_{AP, conc}$, the most influential feature was l_{meter}, with MSE_i/MSE_0 higher than 1 (Figures 6 and 7). This suggests that jump length is a good predictor of these power metrics. Other important features included:

- for $P_{AP, tot}$: F_{AP}, i.e., the time from AP acceleration positive peak to the take-off, underscoring the significance of the concentric phase in determining total antero-posterior power.
- for $P_{AP, conc}$: C_V, u_V, and n_{AP}, i.e., time from minimum to maximum vertical acceleration, mean concentric vertical power, and positive peak AP power, respectively, demonstrating that both power estimates and time periods covering vertical and horizontal directions influence AP power in the concentric phase.

Finally, the analysis of models employing subsets of data (only male/female participants and the dataset with 80 subjects) demonstrated that $P_{AP, tot,}$ and $P_{AP, conc}$ could be reliably estimated in these cases as well. The comparable results in metrics across all three datasets suggest that the estimation of these two power outputs is contingent on dataset size rather than the sex of the subjects.

5. Conclusions

The machine learning solutions that emerged as applicable in this study were all based on a Multi-Layer Perceptron Regressor with significant R^2 [45] and allowed for a homoscedastic estimate of total and concentric antero-posterior mean powers (RMSE = 0.37 W/kg, $R^2 > 0.70$) and a heteroscedastic estimate of the antero-posterior peak power (RMSE = 2.34 W/kg; $R^2 = 0.67$).

Although alternative methodologies, such as deep learning, could be used to enhance parameter estimates, the proposed method offers the advantage of interpretability for coaches and trainers. By linking the estimated parameters to features with biomechanical relevance, the method allows the interpretation of the performance in SLJ. The implementation of this machine learning model into a software tool, like a smartphone app, could enable the quantification of SLJ power outputs, thereby providing a cost-effective, user-friendly, and field-applicable solution. Additionally, this smartphone app could offer the values of the most influential features identified in the PFI analysis, which could assist trainers in determining modifications to enhance jump performance (e.g., emphasizing timing before take-off—F_{AP}). In addition, instructional videos can be made available to facilitate proper smartphone use and feature interpretation.

The proposed solution underscores the importance of jump length, a quantity to be directly measured, as a key feature for power parameter estimation. This finding could lead to the next level of implementation, where the system could operate directly with estimated features and anthropometric data. In this development, methods of jump length estimation (e.g., [26]) can be integrated, thereby enabling power estimates entirely based on the use of inertial sensor signals.

Author Contributions: Conceptualization, B.D.L. and V.C.; methodology, B.D.L.; software, B.D.L.; formal analysis, B.D.L.; investigation, B.D.L.; resources, G.V. and V.C.; data curation, B.D.L.; writing—original draft preparation, B.D.L.; writing—review and editing, B.D.L., G.V., and V.C.; visualization, B.D.L.; supervision, G.V. and V.C.; project administration, G.V. and V.C.; funding acquisition, G.V. and V.C. All authors have read and agreed to the published version of the manuscript.

Institutional Review Board Statement: The study was conducted in accordance with the Declaration of Helsinki and approved by the Internal Review Board of the University of Rome "Foro Italico",

piazza Lauro de Bosis 6, 00135, Rome, Italy (protocol code No. CAR-94/2021/Rev2022, date of approval: 04/05/2022).

Informed Consent Statement: Informed consent was obtained from all subjects involved in the study.

Data Availability Statement: Underlying data are not publicly available due to lack of informed consent for data sharing at the time of collection. Interested researchers may request data, information, or trained models by writing a request to the corresponding author. Matlab scripts generated within the project are available in the following GitHub repository: https://github.com/BeatriceDL?tab= repositories (accessed on 1 January 2025).

Conflicts of Interest: The authors declare that the research was conducted in the absence of any commercial or financial relationships that could be construed as a potential conflicts of interest. The PhD of Dr. Beatrice De Lazzari was co-funded by Go Sport srl.

Appendix A

In the following, Table A1 reports the optimized hyperparameters for each architecture. Tables A2 and A3 include all the models of the power outputs using the male/ female subsets.

Table A1. Type of selected models used for regression. The following columns are reported: model category; hyperparameter options that can be optimized; ranges and options in which hyperparameters can belong to. Names of hyperparameters options are reported as presented by Jupyterlite Notebook.

Model	Hyperparameters	Hyperparameters Options/Ranges
Tree	Criterion Max_depth	{squared_error, friedman_mse, absolute_error, poisson} [1, 100]
RF	N_estimators Criterion Max_features	[100, 500] {squared_error, absolute_error, friedman_mse, poisson} {sqrt, log2, None}
SVR	C Degree Epsilon Kernel	[0.1, 0.5] [1, 2, 3] $[10^{-4}, 10^{-1}]$ {linear, poly, rbf, sigmoid, precomputed}
ADABR	Learning rate Loss N_estimators	$[10^{-10}, 1]$ {linear, squared, exponential} [100, 500]
XGBR	Eta Max_depth N_estimators	$[10^{-3}, 0.5]$ [1, 2, 3] $[10^2, 10^3]$
GBR	Loss N_estimators Criterion Max_features Learning_rate	{squared_error, absolute_error, huber, quantile} (100,150,200,250,300) {friedman_mse, squared_error} {sqrt, log2, None} [0.05, 0.3]
HGBR	Loss Learning_rate Max_iter	{squared_error, absolute_error, gamma, poisson, quantile} [0.05, 0.3] [1, 40]
GPR	Alpha Kernel Optimizer	$[10^{-2}, 10^{-1}]$ {RationalQuadratic(1.0, length_scale_bounds="fixed")+ConstantKernel(1.0, constant_value_bounds="fixed"), RationalQuadratic(1.0, length_scale_bounds="fixed")*ConstantKernel(1.0, constant_value_bounds="fixed"), RationalQuadratic(1.0, length_scale_bounds="fixed"), Matern(1.0, length_scale_bounds="fixed"), Matern(1.0, length_scale_bounds="fixed")*ConstantKernel(1.0, constant_value_bounds="fixed"), Matern(1.0, length_scale_bounds="fixed")+ConstantKernel(1.0, constant_value_bounds="fixed"), RBF(1.0, length_scale_bounds="fixed"), RBF(1.0, length_scale_bounds="fixed")+ConstantKernel(1.0, constant_value_bounds="fixed"), RBF()*ConstantKernel(), ConstantKernel(1.0, constant_value_bounds="fixed") * RBF(1.0, length_scale_bounds="fixed")} {fmin_l_bfgs_b, None}
MLPR	Activation Alpha LayerSize LearningRate Solver	{identity, logistic, tanh, relu} $[10^{-8}, 10^{-1}]$ [1, number_of_selected_features] {constant, adaptive, invscaling} {adam, sgd}

Table A2. List of the best models for each output variable using only the jumps of male subjects as input dataset in grid search optimization, with optimized hyperparameters and mean values of the metrics along the 5-folds.

Output Feature (M)	Model	Hyperparameters	RMSE [W/kg]	MSE [(W/kg)²]	MAE [W/kg]	R²
$P_{TOT, peak}$	MLPR	Activation: logistic Alpha: 10^{-2} LayerSize: 24 LearningRate: invscaling Solver: sgd	5.37	29.7	4.19	0.07
$P_{TOT, conc}$	SVR	C: 0.05 Degree: 1 Epsilon: 0.01 Kernel: sigmoid	1.15	1.41	0.83	0.18
$P_{V, peak}$	RF	N_estimators: 395 Criterion: absolute_error Max_features: None	5.77	34.9	4.49	0.03
$P_{V, conc}$	GBR	Loss: absolute_error N_estimators: 250 Criterion: friedman_mse Max_features: None Learning rate: 0.12	0.96	1.02	0.68	0.09
$P_{AP, peak}$	SVR	C: 2.3 Degree: 1 Epsilon: 0.005 Kernel: sigmoid	2.27	5.25	1.82	0.47
$P_{AP, conc}$	MLPR	Activation: identity Alpha: 10^{-4} LayerSize: 30 LearningRate: invscaling Solver: adam	0.32	0.10	0.26	0.57
$P_{AP, tot}$	MLPR	Activation: identity Alpha: 10^{-5} LayerSize: 35 LearningRate: adaptive Solver: adam	0.35	0.13	0.28	0.59

Table A3. List of the best models for each output feature using only the jumps of female subjects as input dataset in grid search optimization, with optimized hyperparameters and mean values of the metrics along the 5-folds.

Output Feature (F)	Model	Hyperparameters	RMSE [W/kg]	MSE [(W/kg)²]	MAE [W/kg]	R²
$P_{TOT, peak}$	GBR	Loss: huber N_estimators: 200 Criterion: friedman_mse Max_features: sqrt Learning rate: 0.13	4.18	18.1	3.09	0.10
$P_{TOT, conc}$	MLPR	Activation: logistic Alpha: 10^{-1} LayerSize: 4 LearningRate: constant Solver: sgd	0.64	0.42	0.47	0.18

Table A3. *Cont.*

Output Feature (F)	Model	Hyperparameters	RMSE [W/kg]	MSE [(W/kg)^2]	MAE [W/kg]	R^2
$P_{V, peak}$	GBR	Loss: absolute_error N_estimators: 150 Criterion: friedman_mse Max_features: sqrt Learning rate: 0.08	4.36	19.5	3.33	0.11
$P_{V, conc}$	MLPR	Activation: logistic Alpha: 10^{-6} LayerSize: 13 LearningRate: adaptive Solver: sgd	0.65	0.43	0.47	0.18
$P_{AP, peak}$	XGBR	Eta: 0.07 Max_depth: 3 N_estimators: 102	1.89	3.65	1.43	0.59
$P_{AP, conc}$	GPR	Alpha: 10^{-1} Kernel: RBF(length_scale = 1) * 1 ** 2 Optimizer: fmin_l_bfgs_b	0.27	0.07	0.20	0.69
$P_{AP, tot}$	SVR	C: 0.3 Degree: 1 Epsilon: 10^{-3} Kernel: poly	0.26	0.07	0.19	0.71

Names of hyperparameters as reported in Jupyterlite Notebook, where the symbol "*" stands for a multiplication and "**" for the exponentiation.

References

1. Akay, M.F.; Özçiloğlu, M.M.; Bahar, A. Development of Standing Long Jump Distance Prediction Models Using Generalized Regression Neural Network. *ICOLES* **2018**, *6*, 28.

2. Castro-Piñero, J.; Ortega, F.B.; Artero, E.G.; Girela-Rejón, M.J.; Mora, J.; Sjöström, M.; Ruiz, J.R. Assessing Muscular Strength in Youth: Usefulness of Standing Long Jump as a General Index of Muscular Fitness. *J. Strength Cond. Res.* **2010**, *24*, 1810–1817. [CrossRef] [PubMed]

3. Almuzaini, K.S.; Fleck, S.J. Modification of the Standing Long Jump Test Enhances Ability to Predict Anaerobic Performance. *J. Strength Cond. Res.* **2008**, *22*, 1265–1272. [CrossRef] [PubMed]

4. Mann, J.B.; Bird, M.; Signorile, J.F.; Brechue, W.F.; Mayhew, J.L. Prediction of Anaerobic Power From Standing Long Jump in NCAA Division IA Football Players. *J. Strength Cond. Res.* **2021**, *35*, 1542–1546. [CrossRef]

5. Beato, M.; Bigby, A.E.J.; De Keijzer, K.L.; Nakamura, F.Y.; Coratella, G.; McErlain-Naylor, S.A. Post-Activation Potentiation Effect of Eccentric Overload and Traditional Weightlifting Exercise on Jumping and Sprinting Performance in Male Athletes. *PLoS ONE* **2019**, *14*, e0222466. [CrossRef] [PubMed]

6. Zerf, M.; Arab. Kerroum, M.; Bouabdellah, S.B.A. Relationship between Power Strength and Anaerobic Power Index as a Clear Picture of the Effect of Strength Training among Young Soccer Elite Players. *Слобожанський Науково-Спортивний Вісник* **2019**, *2*, 80–85. [CrossRef]

7. Brumitt, J.; Heiderscheit, B.C.; Manske, R.C.; Niemuth, P.E.; Rauh, M.J. Lower Extremity Functional Tests and Risk of Injury in Division Iii Collegiate Athletes. *Int. J. Sports Phys. Ther.* **2013**, *8*, 216–227.

8. Konz, S.M. Vertical Jump and Standing Long Jump Power to Determine Lower Extremity Imbalance and Injury Risk: 2638 Board #161 June 3, 11. *Med. Sci. Sports Exerc.* **2016**, *48*, 735–736. [CrossRef]

9. Sgrò, F.; Mango, P.; Pignato, S.; Schembri, R.; Licari, D.; Lipoma, M. Assessing Standing Long Jump Developmental Levels Using an Inertial Measurement Unit. *Percept. Mot. Ski.* **2017**, *124*, 21–38. [CrossRef] [PubMed]

10. Agar-Newman, D.J.; Klimstra, M.D. Efficacy of Horizontal Jumping Tasks as a Method for Talent Identification of Female Rugby Players. *J. Strength Cond. Res.* **2015**, *29*, 737–743. [CrossRef]

11. Vincent, L.M.; Blissmer, B.J.; Hatfield, D.L. National Scouting Combine Scores as Performance Predictors in the National Football League. *J. Strength Cond. Res.* **2019**, *33*, 104–111. [CrossRef] [PubMed]

12. Hudgins, B.; Scharfenberg, J.; Triplett, N.T.; McBride, J.M. Relationship Between Jumping Ability and Running Performance in Events of Varying Distance. *J. Strength Cond. Res.* **2013**, *27*, 563–567. [CrossRef] [PubMed]

13. Wiklander, J.; Lysholm, J. Simple Tests for Surveying Muscle Strength and Muscle Stiffness in Sportsmen. *Int. J. Sports Med.* **1987**, *8*, 50–54. [CrossRef]

14. Nuzzo, J.L.; McBride, J.M.; Cormie, P.; McCaulley, G.O. Relationship between Countermovement Jump Performance and Multijoint Isometric and Dynamic Tests of Strength. *J. Strength Cond. Res.* **2008**, *22*, 699–707. [CrossRef]

15. Fleck, S.J.; Smith, S.L.; James, C.R.; Vint, P.F.; Porter, J. Relationship of different traininc jumps to ski jump distance: 1043. *Med. Sci. Sports Exerc.* **1992**, *24*, S174. [CrossRef]

16. Harry, J.R.; Krzyszkowski, J.; Chowning, L.D.; Kipp, K. Phase-Specific Force and Time Predictors of Standing Long Jump Distance. *J. Appl. Biomech.* **2021**, *37*, 400–407. [CrossRef] [PubMed]

17. Hickox, L.J.; Ashby, B.M.; Alderink, G.J. Exploration of the Validity of the Two-Dimensional Sagittal Plane Assumption in Modeling the Standing Long Jump. *J. Biomech.* **2016**, *49*, 1085–1093. [CrossRef] [PubMed]

18. Mackala, K.; Stodółka, J.; Siemienski, A.; Ćoh, M. Biomechanical Analysis of Standing Long Jump From Varying Starting Positions. *J. Strength Cond. Res.* **2013**, *27*, 2674–2684. [CrossRef] [PubMed]

19. Szerdiová, L.; Simšik, D.; Dolná, Z. Assessment of Kinematics of Sportsmen Performing Standing Long Jump in 2 Different Dynamical Conditions. *Metrol. Meas. Syst.* **2012**, *19*, 85–94. [CrossRef]

20. Wu, W.F.W.; Porter, J.M.; Brown, L.E. Effect of Attentional Focus Strategies on Peak Force and Performance in the Standing Long Jump. *J. Strength Cond. Res.* **2012**, *26*, 1226–1231. [CrossRef] [PubMed]

21. Hughes, G.T.G.; Camomilla, V.; Vanwanseele, B.; Harrison, A.J.; Fong, D.T.P.; Bradshaw, E.J. Novel Technology in Sports Biomechanics: Some Words of Caution. *Sports Biomech.* **2021**, *23*, 393–401. [CrossRef] [PubMed]

22. Picerno, P.; Camomilla, V.; Capranica, L. Countermovement Jump Performance Assessment Using a Wearable 3D Inertial Measurement Unit. *J. Sports Sci.* **2011**, *29*, 139–146. [CrossRef]

23. Clemente, F.; Badicu, G.; Hasan, U.C.; Akyildiz, Z.; Pino-Ortega, J.; Silva, R.; Rico-González, M. Validity and Reliability of Inertial Measurement Units for Jump Height Estimations: A Systematic Review. *Hum. Mov.* **2022**, *23*, 1–20. [CrossRef]

24. Mascia, G.; De Lazzari, B.; Camomilla, V. Machine Learning Aided Jump Height Estimate Democratization through Smartphone Measures. *Front. Sports Act. Living* **2023**, *5*, 1112739. [CrossRef] [PubMed]

25. White, M.G.; De Lazzari, B.; Bezodis, N.E.; Camomilla, V. Wearable Sensors for Athletic Performance: A Comparison of Discrete and Continuous Feature-Extraction Methods for Prediction Models. *Mathematics* **2024**, *12*, 1853. [CrossRef]

26. De Lazzari, B.; Mascia, G.; Vannozzi, G.; Camomilla, V. Estimating the Standing Long Jump Length from Smartphone Inertial Sensors through Machine Learning Algorithms. *Bioengineering* **2023**, *10*, 546. [CrossRef] [PubMed]

27. Li, Y.; Peng, X.; Zhou, G.; Zhao, H. SmartJump: A Continuous Jump Detection Framework on Smartphones. *IEEE Internet Comput.* **2020**, *24*, 18–26. [CrossRef]

28. White, M.G.; Bezodis, N.E.; Neville, J.; Summers, H.; Rees, P. Determining Jumping Performance from a Single Body-Worn Accelerometer Using Machine Learning. *PLoS ONE* **2022**, *17*, e0263846. [CrossRef]

29. Staacks, S.; Hütz, S.; Heinke, H.; Stampfer, C. Advanced Tools for Smartphone-Based Experiments: Phyphox. *Phys. Educ.* **2018**, *53*, 045009. [CrossRef]

30. Bergamini, E.; Ligorio, G.; Summa, A.; Vannozzi, G.; Cappozzo, A.; Sabatini, A. Estimating Orientation Using Magnetic and Inertial Sensors and Different Sensor Fusion Approaches: Accuracy Assessment in Manual and Locomotion Tasks. *Sensors* **2014**, *14*, 18625–18649. [CrossRef]

31. Rantalainen, T.; Finni, T.; Walker, S. Jump Height from Inertial Recordings: A Tutorial for a Sports Scientist. *Scand. J. Med. Sci. Sports* **2020**, *30*, 38–45. [CrossRef] [PubMed]

32. Owen, N.J.; Watkins, J.; Kilduff, L.P.; Bevan, H.R.; Bennett, M.A. Development of a Criterion Method to Determine Peak Mechanical Power Output in a Countermovement Jump. *J. Strength Cond. Res.* **2014**, *28*, 1552–1558. [CrossRef] [PubMed]

33. McMahon, J.J.; Lake, J.P.; Suchomel, T.J. Vertical Jump Testing. In *Performance Assessment in Strength and Conditioning*; Comfort, P., Jones, P.A., McMahon, J.J., Eds.; Routledge: London, UK, 2018.

34. Dowling, J.J.; Vamos, L. Identification of Kinetic and Temporal Factors Related to Vertical Jump Performance. *J. Appl. Biomech.* **1993**, *9*, 95–110. [CrossRef]

35. Dragomiretskiy, K.; Zosso, D. Variational Mode Decomposition. *IEEE Trans. Signal Process.* **2014**, *62*, 531–544. [CrossRef]

36. Tibshirani, R. Regression Shrinkage and Selection Via the Lasso. *J. R. Stat. Soc. Ser. B (Methodol.)* **1996**, *58*, 267–288. [CrossRef]

37. Pedregosa, F.; Varoquaux, G.; Gramfort, A.; Michel, V.; Thirion, B.; Grisel, O.; Blondel, M.; Prettenhofer, P.; Weiss, R.; Dubourg, V. Scikit-Learn: Machine Learning in Python. *J. Mach. Learn. Res.* **2011**, *12*, 2825–2830.

38. Claudino, J.G.; de Oliveira Capanema, D.; de Souza, T.V.; Serrão, J.C.; Machado Pereira, A.C.; Nassis, G.P. Current Approaches to the Use of Artificial Intelligence for Injury Risk Assessment and Performance Prediction in Team Sports: A Systematic Review. *Sports Med.-Open* **2019**, *5*, 1–12. [CrossRef] [PubMed]

39. Bland, J.M.; Altman, D.G. Statistics Notes: Measurement Error Proportional to the Mean. *BMJ* **1996**, *313*, 106. [CrossRef]

40. Altmann, A.; Toloşi, L.; Sander, O.; Lengauer, T. Permutation Importance: A Corrected Feature Importance Measure. *Bioinformatics* **2010**, *26*, 1340–1347. [CrossRef] [PubMed]

41. Breiman, L. Random Forests. *Mach. Learn.* **2001**, *45*, 5–32. [CrossRef]
42. Fisher, A.; Rudin, C.; Dominici, F. All Models Are Wrong, but Many Are Useful: Learning a Variable's Importance by Studying an Entire Class of Prediction Models Simultaneously. *J. Mach. Learn. Res.* **2018**, *20*, 1–81. [CrossRef]
43. Giavarina, D. Understanding Bland Altman Analysis. *Biochem. Medica* **2015**, *25*, 141–151. [CrossRef]
44. Kendall, M.G. A New Measure of Rank Correlation. *Biometrika* **1938**, *30*, 81–93. [CrossRef]
45. Chicco, D.; Warrens, M.J.; Jurman, G. The Coefficient of Determination R-Squared Is More Informative than SMAPE, MAE, MAPE, MSE and RMSE in Regression Analysis Evaluation. *PeerJ Comput. Sci.* **2021**, *7*, e623. [CrossRef] [PubMed]